UCLA
COMPUTATIONAL AND APPLIED MATHEMATICS

Computation of Flow Noise Via Asymptotic Expansions

Christopher R. Anderson
Karen Pao

July 1993

CAM Report 93-23

Department of Mathematics
University of California, Los Angeles
Los Angeles, CA. 90024-1555

UCLA
COMPUTATIONAL AND APPLIED MATHEMATICS

Computation of Flow Noise Via Asymptotic Expansions

Christopher R. Anderson
Karen Pao

July 1993

CAM Report 93-23

This report has been accepted for the Proceedings of the ASME Symposium on Flow Noise Modeling, Measurement, and Control.

Department of Mathematics
University of California, Los Angeles
Los Angeles, CA. 90024-1555

COMPUTATION OF FLOW NOISE VIA ASYMPTOTIC EXPANSIONS

CHRISTOPHER R. ANDERSON AND KAREN PAO *

Abstract. We develop a numerical method for computing the sound generated by unsteady low speed flows in two space dimensions. Because the acoustics and the fluid flow vary on different time and length scales, direct solutions of the aerodynamic sound generation problem can be computationally difficult. Our approach is to compute the acoustic waves separately from the fluid motion. The procedure is based on an asymptotic decomposition by Majda and Klainermann, who represent aerodynamic sound as a correction to the incompressible component of a fluid flow. The acoustic correction satisfies a system of partial differential equations; our work focuses on the numerical solution of these acoustical equations, and a numerical technique for coupling the acoustics and the incompressible flow. The sounds generated by various configurations of vortices are computed.

1. Introduction. One of the primary problems in the computation of acoustic signals induced by low Mach number fluid motion is the presence of different time and spatial scales. By definition, low Mach number flows are characterized by the situation that the fluid velocity is much less than the speed of sound, $v_{fluid} << c$. The implication for computation is that if one solves the compressible equations, the timestep must be chosen to resolve features associated with the acoustics and this is much smaller than a timestep necessary to resolve features of the fluid motion. Of course, if one ignores the acoustics and solves the incompressible equations instead, then one can then use larger timesteps. The spatial scale of the acoustic waves can also be much larger than the fluid structure which generates them. Sound is related to vorticity dynamics, and the scale of the vortical structures is often much smaller than the acoustic wavelength. To overcome the problems caused by these disparities in scale it is a natural idea to try to compute the fluid motion using the incompressible equations and then recover the acoustics by an auxiliary computation. This is the basic idea behind approaches to aeroacoustics suggested by, for example, Lighthill (1952) and Powell (1964). In our work we have undertaken to develop a systematic approach to computing acoustic signals based on the idea of separate incompressible flow/acoustic computations.

The theoretical foundation for the work is provided by an asymptotic expansion due to Majda and Klainerman (1982). In this decomposition the compressible flow field is represented as an incompressible flow plus an acoustical correction. Majda and Klainermann show that the acoustical correction satisfies a system of linear hyperbolic equations whose coefficients are functions of the incompressible flow variables. In this paper we summarize the equations of the Majda-Klainerman decomposition, our numerical procedure for solving them, and then present some sample results.

2. Formulation. We briefly outline the derivation of the acoustics equations described in Majda and Klainermann (1981). Consider the equations of isentropic com-

* Department of Mathematics, UCLA, Los Angeles, California, 90024
Research Supported by DARPA contract #N00014-92-J-1890

pressible flows

$$\rho_t + v \cdot \nabla \rho + \rho \nabla \cdot v = 0, \tag{1}$$

$$\rho(v_t + v \cdot \nabla v) + \nabla p = 0, \tag{2}$$

with initial conditions

$$\rho(x,0) = \rho_0(x), v(x,0) = v_0(x).$$

The pressure and the density are related by the equation of states

$$p = p(\rho).$$

Here we shall assume that the fluid is an ideal gas, that is,

$$p = \rho^\gamma,$$

where γ is the ratio of the specific heats.

We shall non-dimensionalize these equations by a change of variables: scale the variables by $\rho_m = \max_x \rho_0(x)$ and $|v_m| = \max_x |v_0(x)|$, and let

$$\tilde{v} = \frac{v}{|v_m|}, \tag{3}$$

$$\tilde{\rho} = \frac{\rho}{\rho_m}, \tag{4}$$

$$x' = \frac{x}{x_m}, \qquad t' = \frac{|v_m| t}{x_m}. \tag{5}$$

Setting $x_m = 1$, dropping the ˜ variables and reverting to the old variables, we have

$$\begin{aligned} p_t + v \cdot \nabla p + p \nabla \cdot v &= 0 \\ v_t + v \cdot \nabla v + \frac{1}{M^2} \nabla p &= 0 \end{aligned} \tag{6}$$

with initial conditions

$$p(x,0) = p_0(x), v(x,0) = v_0(x).$$

Here M is the Mach number, defined as

$$M = \frac{\gamma^{1/2} |v_m|}{(dp/d\rho)|_{\rho_m}{}^{1/2}}. \tag{7}$$

The equations of inviscid, incompressible flow are

$$\begin{aligned} v_t^\infty + v^\infty \cdot \nabla v^\infty + \nabla p^\infty &= 0, \\ \nabla \cdot v^\infty &= 0, \end{aligned} \tag{8}$$

with initial conditions

$$p^\infty(x,0) = p_0^\infty(x), v^\infty(x,0) = v_0^\infty(x).$$

It has been shown (for example, in Majda and Klainermann (1982)) that, as M goes to zero in (6), we obtain (8) . We are interested in the case $M \ll 1$.

Majda and Klainermann (1981), (1982) have shown that

$$p = P^0 + M^2(p^\infty + p_1) + O(M^3), \tag{9}$$

$$v = v^\infty + Mv_1 + O(M^2), \tag{10}$$

where (p_1, v_1) satisfy

$$v_{1t} + v^\infty \cdot \nabla v_1 + v_1 \cdot \nabla v^\infty + \frac{1}{M}\nabla p = 0, \tag{11}$$

$$p_{1t} + v^\infty \cdot \nabla p_1 + \frac{1}{M}\nabla \cdot v_1 = -(p_t^\infty + v^\infty \cdot \nabla p^\infty), \tag{12}$$

with initial conditions

$$\begin{aligned} p_1(x,0) &= p_1^0(x) - p^\infty(x,0), \\ v_1(x,0) &= v_1^0(x). \end{aligned}$$

Note that when the incompressible flow is identically zero, the equations above are reduced to the classical wave equations

$$\begin{aligned} v_{1t} + \frac{1}{M}\nabla p_1 &= 0, \\ p_{1t} + \frac{1}{M}\nabla \cdot v_1 &= 0, \end{aligned}$$

with the appropriate initial conditions.

An assumption in the derivation of these equations is that the wave lengths of the acoustic waves represented by the asymptotics must be large compared to the size of the acoustic source. To see that, substitute the expansions (9) and (10) into the scaled compressible Euler's equation (6). In order to balance the the $O(1)$ terms and obtain the incompressible Euler's equation (8), we must have

$$\nabla p_1 \sim O(M).$$

This implies that the acoustic pressure cannot change much over a distance of $O(1/M)$. Moreover, the asymptotic expansions do not provide a mechanism of feedback of acoustics to the fluids. Acoustic computations based on these expansions should be employed only in situations where there is no interaction between the acoustics and the incompressible fluid flow, and where the high frequency components are not significant.

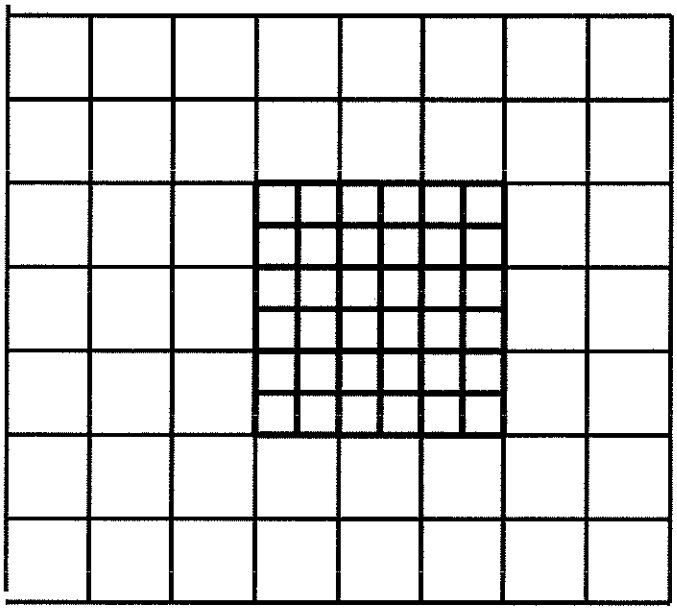

FIG. 1. *The layout of the grids used in the computations*

3. Numerical Implementation. The scaled perturbations p_1 and v_1 give us the acoustics in the fluid flow, and thus our task is to solve the system (11) and (12). In order to solve (11) and (12), we first need to obtain the incompressible variables v^∞ and p^∞. In our computations, the incompressible flow field is provided by a discrete vortex method (Chorin, 1973). While the method is Lagrangian, and computational variable is the vorticity (the curl of the velocity), it is possible to extract from the solutions the values of the flow variables v^∞, p^∞ on a grid. We then solve the system (11) and (12) using a finite difference method. The finite difference method implemented is a two-dimensional unsplit upwind method described in Colella (1990). First-order absorbing boundary conditions described in Engquist and Majda (1977) are used to represent an infinite domain by a finite one. The source for the acoustic equations is assosociated with the vortical structures of the incompressible flow. To resolve this source, a small, finer grid is used. A larger, as well as coarser grid is used to resolve the sound waves emanating from the source region. This large grid is placed over the finer grid as shown in figure 1. Since the incompressible flow does not change appreciably over the time interval in which the acoustics are resolved, interpolation is used to obtain necessary incompressible data. The time marching scheme is depicted in figure 2.

4. Numerical Experiments. We present the results of three different computations. They are all associated with the evolution of different configurations of vorticity. We discuss the sound generated by a pair of rigidly rotating point vortices, by a finite vortex sheet, and by a collection of vortices that simulate a wake.

4.1. Sound Generation by Two Rigidly Rotating Vortices. In this problem, two point vortices of the same sign and strength κ are placed at $(-a, 0)$ and $(a, 0)$

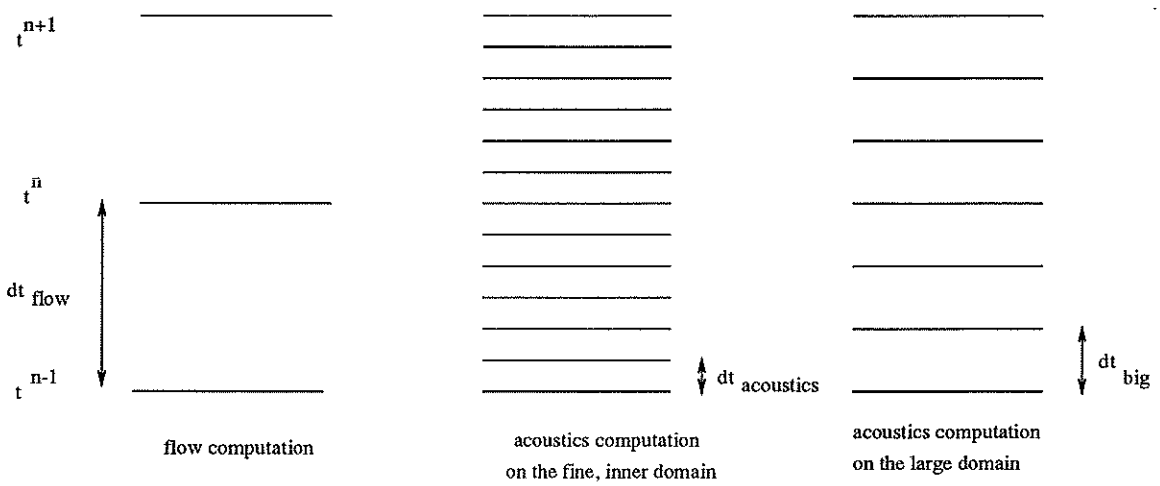

FIG. 2. *The different time steps for the flows computations and the acoustics computations on the large and the small domains.*

initially. The vortices will traverse along the circle $r = a$ at the rate of $\theta_t = \frac{\kappa}{4\pi a^2}$. We set $a = 0.5$. In the acoustics computations, we let $c = 1.0$ be fixed. The values of $\kappa = 0.1, 0.25, 0.5$, corresponding to Mach numbers of $0.19, 0.48, 0.95$, are used. An inner region of $[-4, 4] \times [-4, 4]$ with a 256×256 grid and a large region of $[-8, 8] \times [-8, 8]$ with a 128×128 grid are used. We have computed the evolution of the two vortices *in conjunction* with the acoustics on the fine grid, at a time step of $\triangle t = 0.02$. The computation on the large region is done every 4 steps. Figures 3 – 5 show the scaled pressure at a point in the far field for the various Mach numbers as well as the corresponding spectra.

All these computations show the same features: a large amplitude pressure wave due to initialization, followed by low frequency waves. These computations show that our numerical method does not break down for Mach numbers near 1, although our model does not take possible fluid-acoustics interaction, in particular, at Mach numbers near 1, into consideration. The characteristic frequencies correspond to the respective rotational frequencies of the vortices: when the two vortices have rotated half way around the circle, the vortical configuration becomes identical to the initial one, thus the characteristic frequency of the sound generated by the two vortices should be *twice* the characteristic frequency of the vortical configuration, and that is what we have observed. One can discern a very small high frequency component riding on the low frequency waves in all computations; this effect is slightly more pronounced in the lower Mach number experiments. We suspect that this is an error due to the limitations of the sizes of the computational domain, an artifact of our numerical method. With improvements in computational procedure (which we are investigating) we expect that they can be even further reduced.

4.2. Sound Generation by a Finite Vortex Sheet. Next we compute the sound generated by a finite vortex sheet. This sheet of vorticity is represented by

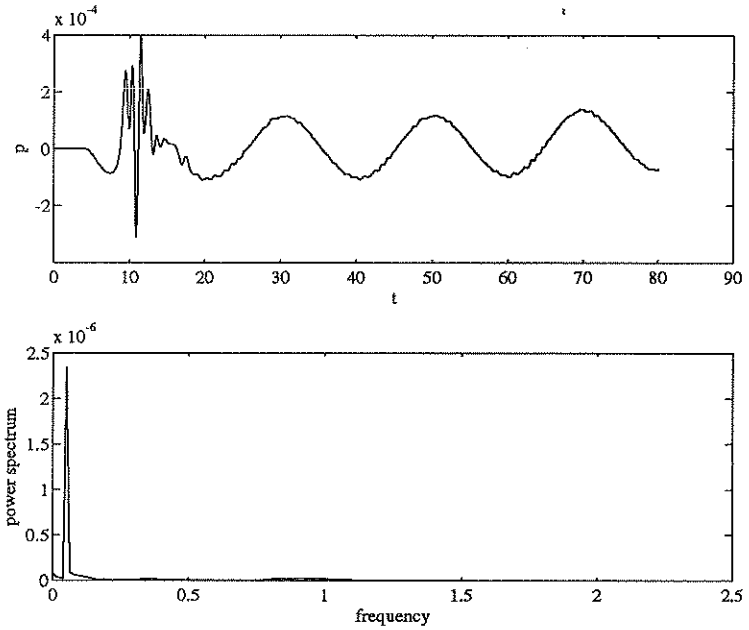

FIG. 3. *Acoustic pressure and power spectrum for* $M = 0.95$, *near the point* $(8, 8)$.

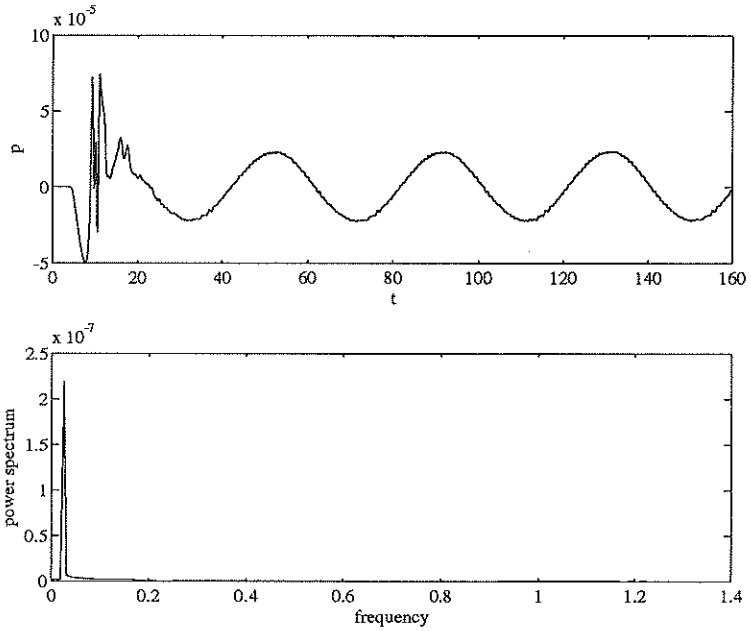

FIG. 4. *Acoustic pressure and power spectrum for* $M = 0.48$, *near the point* $(8, 8)$.

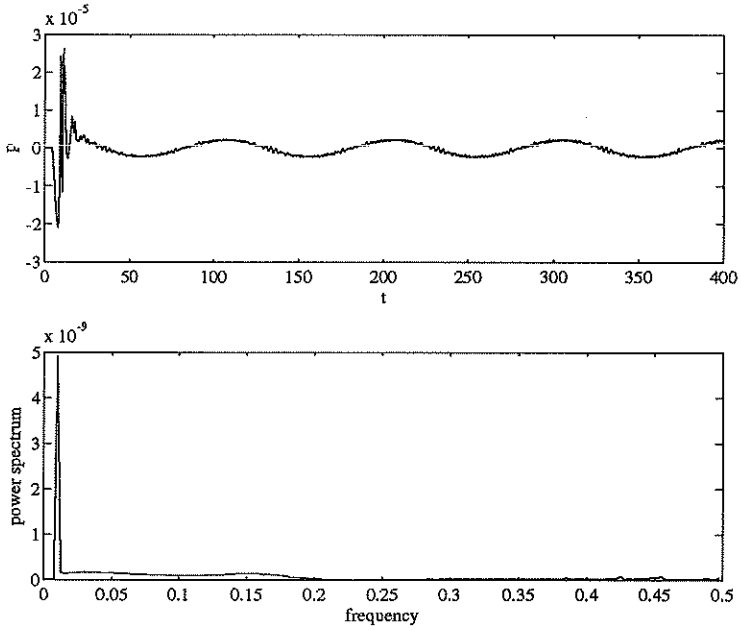

FIG. 5. *Acoustic pressure and power spectrum for* $M = 0.19$, *near the point* $(8, 8)$.

placing N vortex blobs of radius δ of strength

$$\frac{1}{N} \cdot \begin{cases} 0, & |x| > \frac{3}{8} \\ 1, & |x| < \frac{1}{4} \\ 10(8x-3)^3 - 15(8x-3)^4 + 6(8x-3)^5, & -\frac{3}{8} \le x \le -\frac{1}{4} \\ 10(-1-8x)^3 - 15(-1-8x)^4 + 6(-1-8x)^5, & \frac{1}{4} \le x \le \frac{3}{8} \end{cases}$$

on the interval $[-1/2, 1/2]$ along the x-axis. The ends of the vortex sheet roll up into two concentrated vortices. These vortices then precess in a counterclockwise direction. With $\delta = 0.25$ we discretize the sheet into $N = 100$, $N = 200$ and $N = 400$ vortices. The acoustic pressure is computed as a function of time at a fixed point in space. Sample results for $N = 100$ are given in Figure 6 which shows the pressure at $(8, 8)$ as a function of time and its spectrum. Two major components in the acoustic pressure are produced by this configuration of vortices. The main component has a peak frequency of about 0.25; the other, a much smaller component, has a peak frequency of about 0.2 The main component is produced by the rollup of the tips into two concentrated vortices, while the small component is due to the precession of the two composite vortex structures.

What we find particularly interesting about this test problem is that the behavior of the acoustic signal reflects the accuracy of the vortex simulation. Our past experiences have shown us that it is often difficult to tell, by observing the positions of the individual blobs, whether enough vortex blobs have been used in a simulation. This experiment shows that it is possible to use the acoustical signals due to a vortical configuration to determine the accuracy of the vortex motion simulation. For example, in the test problem here, using 100 blobs to represent the vortex sheet is not sufficient to simulate

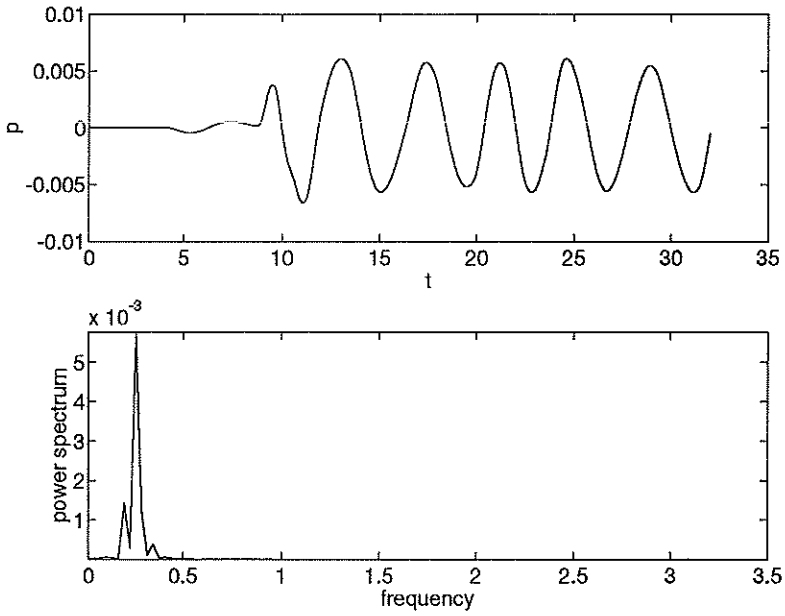

FIG. 6. *Acoustic pressure and power spectrum near the point* $(8,8)$. *Here* $N = 100$.

accurately the motion of the sheet, while using 200 vortex blobs seem to improve the resolution of the vortex simulation, as the acoustic signal for $N = 200$ and $N = 400$ are very similar. This suggests that using 200 vortex blobs of radius 0.25 should be sufficient to resolve the motion of the vortex sheet.

For a fully resolved vortex sheet, the precession of two large composite vortices does not go on forever–they merge and form a single composite structure. This is seen in the results with $N = 200$. With this number of vortices the two composite vortices have essentially merged by $T = 19.2$, while for $N = 400$, the merger has occurred by about $T = 22.4$. By contrast, for $N = 100$, the two composite vortices have barely begun to merge at $T = 28.8$.

This difference in accuracy is reflected by the acoustic pressure associated with the individual runs. Figure 7 shows the acoustic pressure near $(8,8)$ up to $T = 48$ for these three different N's. For $N = 200$ and $N = 400$, the pressure drops significantly around $T = 28$ and $T = 29$, respectively. There is a delay of about 8 time units from the approximate merge time.

This drop in pressure can be understood by considering the effect of merger upon the acoustic source strength. Once the vortices have merged, the core is more or less a radially symmetric distribution of vorticity. The vortices are moved by the inviscid Euler's equation in 2-D, which, in vorticity formulation, is

$$\frac{\partial \omega}{\partial t} + v \cdot \nabla \omega = 0, \tag{13}$$

The term $v \cdot \nabla \omega$ is very small, since the vorticity in the core is essentially radially symmetric. Equation (13) then implies that $\frac{\partial \omega}{\partial t}$ is also very small. Aerodynamic sound

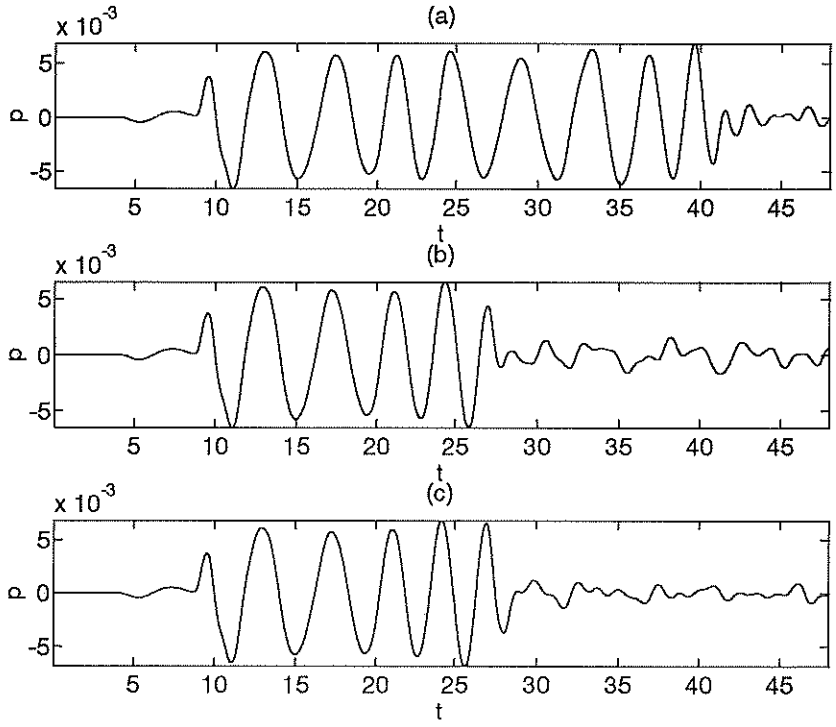

FIG. 7. *Acoustic pressure as a function of time, computed using* $\delta = 0.25$ *and various numbers of vortices. (a)* $N = 100$*; (b)* $N = 200$*; (c)* $N = 400$

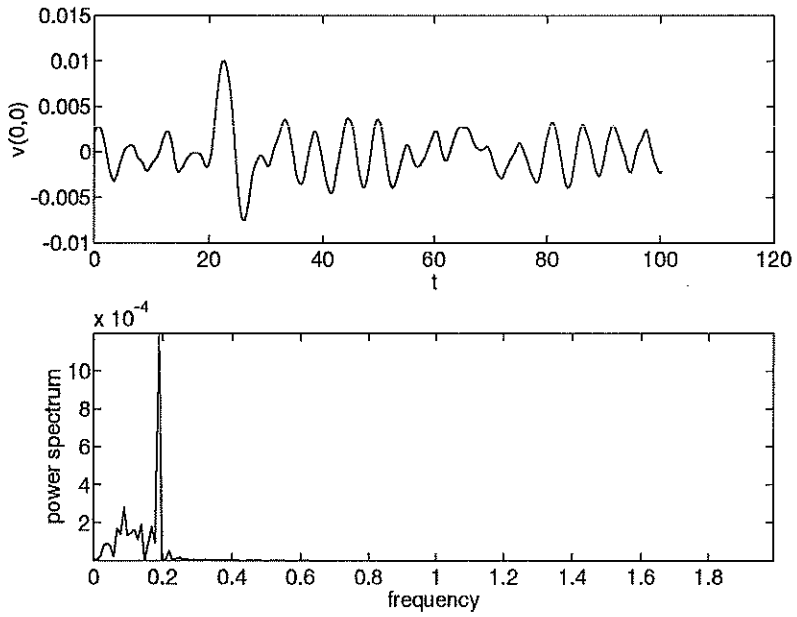

FIG. 8. *Top: the time evolution of the horizontal flow velocity. Bottom: the power spectrum of the velocity evolution.*

is due to the change of vorticity in time (see Möhring (1978)). Thus, upon merging, the source of sound is diminished. This information is then propagated to the point of observation, about 8 length units away from the source, at the sound speed of $s = 1$, and thus the delay time. Our result agrees qualitatively with that of Hardin and Lamkin (1986).

4.3. Sound Generation by a Wake Simulation. We compute the sound generated by a configuration of vortices simulating a finite vortex street. See Anderson (1993) for details of this simulation. This experiment is different from the other two numerical experiments, in that a dipole source of sound is expected.

Figure 8 shows the vertical flow velocity at the origin in the course of the acoustic computation. Spectral analysis shows that this frequency peaks at 0.2. This is the "characteristic frequency" of the flow, and we expect the main component of the acoustic waves generated by the flow to have the same frequency. In the acoustics computation, we let the vortices evolve up to $T = 50$ before starting the acoustics calculation. Homogeneous initial conditions are assumed for the acoustic variables. We compute the acoustics on the region $[-16, 48] \times [-32, 32]$, with a grid of 256×256. We set the sound speed to 2.0, and the Mach number is found to be $M = 0.79$. Substepping and interpolation in time are used; the vortex motions are advanced at a timestep of 0.1, while the acoustics is computed with a timestep of 0.025.

Figure 9 shows the acoustic pressure contours at $T = 100$ after the acoustic calculations have been started. Wavelike structures are propagated out of the source region, while complicated structures can be seen in the source region. Doppler effect is ob-

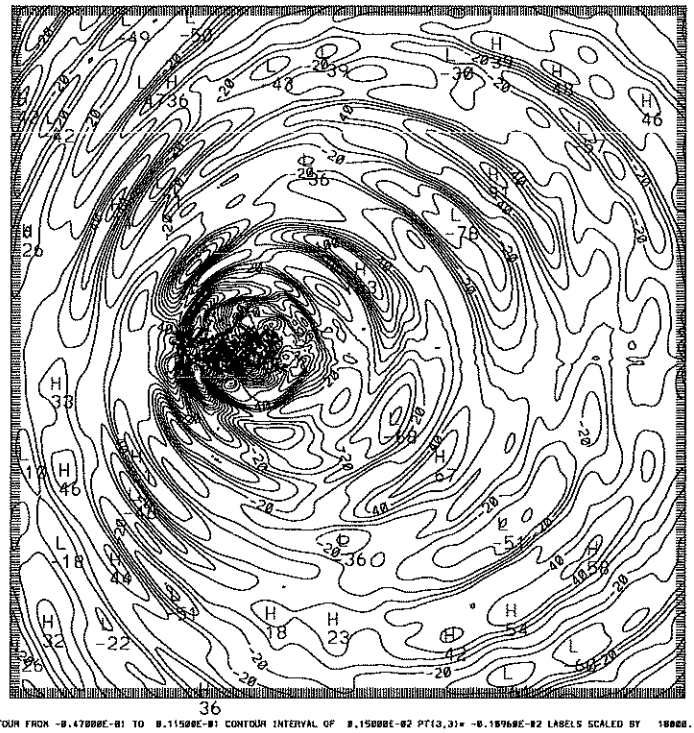

FIG. 9. *Acoustic pressure contour at* $T = 100$

served; the waves are more tightly bunched up in the upstream. The waves are mainly emanated from above and below the injection sites, with very little from directly downstream. The newly born waves are then advected downstream. Again, we examine the acoustic pressure as a function of time at various points. Figures 10 and 11 show the pressure evolutions and the corresponding spectra at an upstream point and a downstream point, respectively. The structure of the sound here is much more complicated than in the previous test problems. There is a broader distribution of frequencies, peaking, in all cases, at 0.2. No harmonics of this base frequency are observed.

5. Conclusions and Future Work. This investigation was begun in an effort to assess the feasibility of computing the acoustic signal of low Mach number flows by using a general incompressible fluid/acoustic correction approach. The computational results show that this approach can be used, and that the approach may be a useful alternative to computations which utilize the compressible equations.

Many improvements of the current algorithm can be made. For example, more sophisticated grid composition techniques can be incorporated into our method. Methods such as composite grid (CMPGRD) (see Brown *et. al.* (1990)) or adaptive mesh refinement (AMR) (see, for example, Berger and Oliger (1984)) may be used in the acoustics calculations, the incompressible computations, or both. A large portion of computing time is spent on solving the acoustic equations on the fine, inner grid. The acoustic computations can be done more efficiently if the fine-structured acoustic source can be represented on the coarse grid. We can then take advantage of the large wavelengths

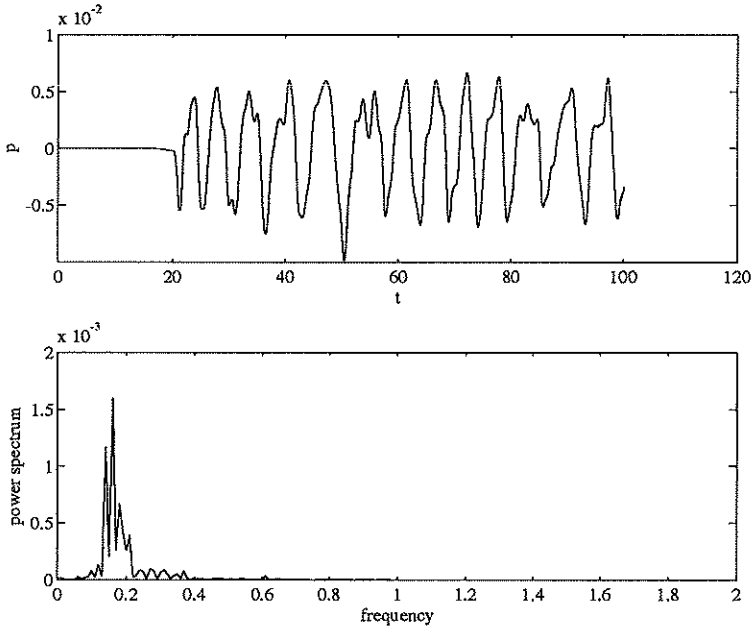

FIG. 10. *Acoustic pressure and power spectrum near* $(-12, 32)$.

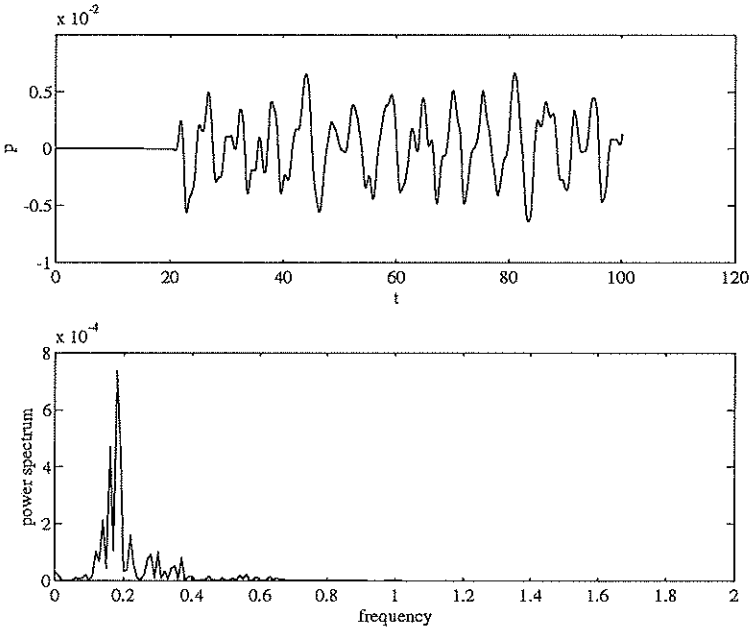

FIG. 11. *Acoustic pressure and power spectrum near* $(48, 32)$.

of the resulting sound waves, and compute the acoustics on the coarse grid only. There is also the extension of the approach to problems in which boundaries are present.

For flows with no boundaries, our technique can be easily modified to compute sound generation in 3-D flows, since the asymptotic expansions are valid for any number of space dimensions. The usefulness of our technique will be closely linked to the availability of three dimensional incompressible data. Supercomputing techniques will be necessary in three-dimensional computations.

REFERENCES

[1] Anderson, C. R., "A Finite Vortex Sheet Model," UCLA Computational and Applied Mathematics Report 93-01 (1993)

[2] Berger, M. J., and Oliger, J., "Adaptive Mesh Refinement for Hyperbolic Partial Differential Equations," *Journal of Computational Physics*, vol. 53, pp. 484-512 (1984)

[3] Brown, D. L., Chesshire, G., Henshaw, B., *Getting Started with CMPGRD: Introductory User's Guide and Reference Manual*, Los Alamos National Laboratory Technical Report LA-UR-90-3729 (1990)

[4] Chorin, A. J., "Numerical Study of Slightly Viscous Flow," *Journal of Fluid Mechanics*, vol. 57, pp. 785-796 (1973).

[5] Colella, P., "Multidimensional Upwind Methods for Hyperbolic Conservation Laws," *Journal of Computational Physics*, vol. 87, pp. 171-200 (1990).

[6] Engquist,B., Majda, A., "Absorbing Boundary Conditions for the Numerical Simulatin of Waves," *Mathematics of Computation*, vol. 31, pp. 629-651 (1977).

[7] Hardin, J. C., Lamkin, S. L., "Computational Aeroacoustics: Present Status and Future Promise," *Proceedings of the IUTAM Sumposium on Aero- and Hydro-Acoustics*, pp. 253-259 (1986).

[8] Lighthill, M.J., "On Sound Generated Aerodynamically," *Proceedings of Royal Society*,vol. A 211, pp. 564-587 (1952).

[9] Majda, A., Klainermann, S., "Compressible and Incompressible Fluids," *Communications in Pure and Applied Mathematics*, vol. 35, pp. 629-651 (1982).

[10] Majda, A., *Compressible Fluid Flow and Systems of Conservation Laws*, Springer-Verlag, New York, 1981

[11] Möhring, W., "On Vortex Sound at Low Mach Number," *Journal of Fluid Mechanics*, vol. 85, pp. 685-691 (1978).

[12] Mueller, E., Obermeier, "Vortex Sound," *Proceedings of the IUTAM Symposium on Fundamental Aspects of Vortex Motion*, pp. 43-51 (1988).

[13] Powell, A., "Theory of Vortex Sound," *Journal of the Acoustical Society of America*, vol.36, pp. 177-195 (1964).